Ab initio study of symmetric tilt boundaries in ZnO

Fumiyasu Oba, Shigeto R. Nishitani, and Hirohiko Adachi
Department of Materials Science and Engineering, Kyoto University, Sakyo, Kyoto 606-8501, Japan

Isao Tanaka
Department of Energy Science and Technology, Kyoto University, Sakyo, Kyoto 606-8501, Japan

Masanori Kohyama and Shingo Tanaka
Department of Materials Physics, Osaka National Research Institute, Agency of Industrial Science and Technology, 1-8-31 Midorigaoka, Ikeda, Osaka 563-8577, Japan

(Received 5 September 2000; published 9 January 2001)

The atomic and electronic structure of the $[0001]/(\overline{1\,2}\,3\,0)$ $\Sigma=7$ symmetric tilt boundary in ZnO has been investigated by an *ab initio* plane-wave pseudopotential method within the local-density approximation. Two types of equilibrium geometries are obtained with similar boundary energies. Atomic arrangement is largely reconstructed to vanish dangling bonds in one configuration, whereas the other shows small bond distortion but has dangling bonds at the boundary core. The balance between the energies for deforming atomic arrangements and vanishing dangling bonds should be significant in determining the boundary energies. The electronic structure of the grain boundaries is discussed with a special interest in the relationship with the bond disorder. Owing to the bond distortion and/or the presence of the dangling bonds, localized states form mainly at the lower valence band and the bottom of the upper valence band. On the other hand, the electronic states in the vicinity of the band gap are not significantly affected by the bond disorder. Deep electronic states are not generated in the band gap even for the configuration with dangling bonds. This behavior can be generally explained by the band structure intrinsic to ZnO.

DOI: 10.1103/PhysRevB.63.045410 PACS number(s): 73.20.Hb, 71.20.Nr, 68.35.Ct

I. INTRODUCTION

Grain boundaries have attracted much attention due to the significant roles in the mechanical and electrical properties of polycrystalline materials. The variety of the atomic arrangement, chemical composition, and electronic structure of the grain boundaries, however, has made it difficult to access the microscopic origins of the boundary-induced properties in general. It has therefore been required to investigate simple boundaries such as the coincidence site lattice[1] (CSL) boundaries systematically. CSL boundaries are often observed in chemical-vapor-deposited films of semiconductors such as Si and SiC.[2,3] On the other hand, they are not necessarily representative in sintered materials. However, the local atomic and electronic structure of the CSL boundaries should have features common to arbitrary boundaries. The systematic knowledge of the CSL boundaries is therefore useful in understanding the atomic and electronic structure that governs macroscopic properties originating from boundary regions. For metal oxides, CSL boundaries have been investigated both experimentally[4–10] and theoretically[10–25] in order to elucidate the atomic structure. Recently, the electronic structure has been revealed for some CSL boundaries likewise.[22–25]

In the present study, we investigate the atomic and electronic structure of the $[0001]/(\overline{1\,2}\,3\,0)$ $\Sigma=7$ symmetric tilt boundary in ZnO by an *ab initio* plane-wave pseudopotential method. Grain boundaries in ZnO are interesting especially for the nonlinear current-voltage characteristics, which are widely utilized as varistors.[26–28] The origin of the characteristics is attributed to the double Schottky barrier based on the interfacial electronic states.[29,30] In ZnO varistors, deep interfacial states have been observed at 0.6–1.0 eV below the bottom of the conduction band.[31–35] A number of reports on the nonlinear properties suggest that the formation of the interfacial electronic states is related to the presence of some impurities and/or excessive oxygen at the grain boundaries.[36–44] However, it should be significant to understand the electronic structure originating from the deformed atomic arrangements at the grain boundaries themselves, differentiating from the extrinsic effects by the impurities and the defects associated with the oxygen excess. For this purpose, we opt to investigate the stoichiometric configurations of the $\Sigma=7$ symmetric tilt boundary in ZnO.

We have previously modeled the $\Sigma=7$ boundary using empirical interatomic potentials.[25] Two types of equilibrium geometries with and without dangling bonds were found to have the lowest grain-boundary energies of similar magnitude. Although the empirical potentials were confirmed to reproduce the bulk properties of ZnO well, there may have been some systematic errors on the boundary geometries and energies.

The first objective of the present study is the evaluation of the boundary geometries and energies in a quantitatively reliable manner based on the *ab initio* method. We eventually find that the equilibrium geometries and energies of the $\Sigma=7$ boundaries of ZnO obtained by the empirical method are qualitatively the same as those obtained by the present *ab initio* method.

The second objective is the elucidation of the effects of the bond disorder on the electronic structure. This is essential

TABLE I. Calculated lattice constants and internal parameter. Deviations from the experimental ones are shown in parentheses.

		Calculated	Experimental[a]
Lattice constants	a (Å)	3.2214 (−0.9%)	3.2507
	c (Å)	5.2031 (−0.1%)	5.2083
Internal parameter	u (frac.)	0.3790 (−0.9%)	0.3825

[a]Reference 53.

to bridge the boundary-induced electrical properties and the atomic arrangements. As a consequence, we find that the electronic states in the vicinity of the band gap are not significantly affected by bond distortion and the presence of dangling bonds. Deep electronic states are not recognized in the band gap even for the configuration with dangling bonds. These results can be generally explained by the band structure intrinsic to ZnO. Deep interface states observed for ZnO varistors should not be attributed solely to bond disorder at stoichiometric boundaries.

II. METHODOLOGY

The *ab initio* calculations were performed using a plane-wave pseudopotential method[45] within the local-density approximation (LDA).[46] The self-consistent total energy in the ground state was obtained by the conjugate-gradient electronic minimization technique,[47] which has been reported to be very efficient for semiconducting/insulating large systems.[48] Atomic positions were iteratively relaxed according to the Hellmann-Feynman force[49] to achieve the optimum geometry.

Troullier-Martins-type pseudopotentials[50] were constructed for neutral Zn and O atoms. The valence electron configurations of $(3d)^{10}(4s)^2(4p)^0$ and $(2s)^2(2p)^4$ and the cutoff radii of 2.34 bohr (1.24 Å) and 1.35 bohr (0.71 Å) were chosen for Zn and O, respectively. These pseudopotentials were used in the Kleinman-Bylander form[51] with the local components of *s* for Zn and *p* for O.

To begin with, we made calculations for the perfect crystal of ZnO to check the applicability of the pseudopotentials. The lattice constants and internal parameter were optimized for the four-atom primitive cell with a plane-wave cutoff energy of 100 Ry (1360 eV) and six special **k** points in the irreducible part of the Brillouin zone.[52] The results are listed in Table I. The calculated values show small deviations from the experimental ones. For this optimized geometry, eigenstates were calculated at 125 **k** points in the irreducible part of the Brillouin zone. The density of states (DOS) was then obtained by substituting Gaussian functions of 0.5 eV full width at half maximum (FWHM) for the eigenstates. The shape of the DOS, which will be shown later in Fig. 4, was confirmed to be very similar to those reported.[25,54,55]

For the calculation of the $[0001]/(\bar{1}\,\bar{2}\,3\,0)$ $\Sigma=7$ symmetric tilt boundary, the geometries modeled in our previous study[25] were employed as initial configurations. We calculated the equilibrium geometries using empirical potentials that are composed of the long-range electrostatic potential with formal ionic charges and the short-range two-body potentials in the Buckingham form.[56] As a result, some types of equilibrium configurations were obtained with different translation states of the two half-crystals. Among them, we chose two configurations with the lowest and the second lowest boundary energies as the initial configurations in the present study. The atomic structures are shown in Fig. 1. Boundary *A* was obtained with the translation states of 0.5 and 0.41 in fraction of the unit boundary lengths for the *x* and *y* directions, respectively. The translation in the *z* direction, which corresponds to the volume expansion normal to the interface, was 0.6 Å. The boundary energy was calculated to be 1.37 J/m^2 by the empirical method. In the $[000\bar{1}]$ view, the bulk region of the wurtzite structure looks like a sequence of sixfold-coordinated channels, whereas the boundary core structure is constructed by a sequence of fourfold- and eightfold-coordinated channels. All of the atoms have complete fourfold coordination of the first nearest neighbors. In other words, there are no dangling bonds in this boundary.

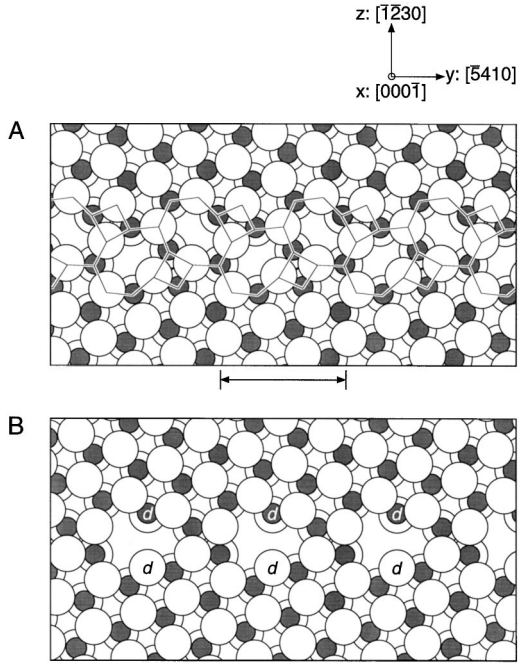

FIG. 1. Equilibrium boundary geometries calculated by the empirical method. The scale indicates the periodicity unit of the boundary. The filled and open circles denote Zn and O atoms, respectively. In the $[000\bar{1}]$ view, three of the four basal planes in the ZnO unit cell can be seen in the order of O-Zn-O. For the boundary *A*, core structure is described as a sequence of fourfold- and eightfold-coordinated channels. For the boundary *B*, atoms possessing dangling bonds are labeled with *d*.

Boundary *B* has the translation states of 0.5, 0 in fraction, and 0.9 Å for the *x*, *y*, and *z* directions, respectively. At the boundary core, there are large open channels along the [0001] direction. Some atoms adjacent to the channels have lost one of the first nearest neighbors, which are labeled *d* to signify dangling bonds. The number of dangling bonds is four per unit boundary area. Despite the presence of the dan-

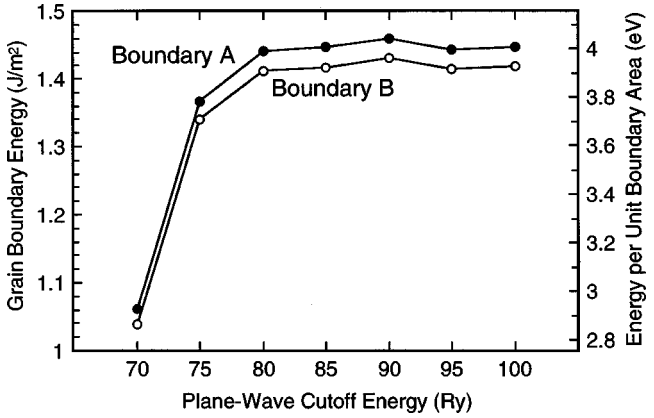

FIG. 2. Grain-boundary energies as a function of plane-wave cutoff energy. The right-hand ordinate indicates the energy per unit boundary area, i.e., energy per boundary in the supercell.

gling bonds, the boundary energy was calculated to be only 0.11 J/m^2 higher than that of boundary *A* by the empirical method.

For these boundaries, we constructed 80-atom supercells that contain two identical boundaries to match three-dimensional periodic boundary conditions, as will be shown later in Fig. 3. The supercells have the glide-plane symmetry with respect to the *x*-*z* plane. First the atomic positions in the supercells were redetermined by the empirical calculation under three-dimensional periodic boundary conditions. In these calculations, the relaxation for twelve atoms located between the two boundaries was restricted within the rigid-body translation parallel to the *y* direction. The resultant geometries were very similar to the ones shown in Fig. 1. The cell dimensions and the atomic coordinates in the *x* direction were then changed on the basis of the lattice constants and internal parameter optimized by the *ab initio* method, which are shown in Table I.

For the calculation of the 80-atom boundary supercells, a plane-wave cutoff energy of 100 Ry and 1 **k** point at the center of the irreducible part of the Brillouin zone, which is one quarter in volume, were employed. In order to test the convergency with respect to cutoff energy, calculations with the cutoff energies ranging from 70 to 95 Ry were also done. Figure 2 shows the grain-boundary energies as a function of cutoff energy, which were calculated as half the difference between the total energy of the boundary supercell and 20 times the total energy of the bulk primitive cell. With the cutoff energy of 100 Ry, the boundary energies are satisfactorily converged: the cutoff energies more than 80 Ry give the convergence within 0.02 J/m^2 (0.0012 eV/Å^2) or 0.05 eV per boundary in the supercell.

The geometry optimization was performed under the condition that the relaxation for twelve atoms located between the two boundaries in the supercells was restricted within the rigid-body translation parallel to the *y* direction, as in the empirical calculations for the construction of the initial configurations. The optimization procedure was truncated when all the residual forces for the unrestricted atoms became less than 0.2 eV/Å.

In order to discuss the one-electron structure, eigenstates were calculated at nine **k** points in the irreducible part of the Brillouin zone for the boundary supercells. In this case, the plane-wave cutoff energies of 80 Ry were employed because of computational economy: with the cutoff energy, the energies of eigenstates at the Γ, *A*, *H*, *K*, *L*, and *M* points for the bulk primitive cell converged within 0.006 eV relative to the results with the cutoff energy of 100 Ry, and the grain-boundary energies per unit boundary area converged within 0.05 eV as shown in Fig. 2.

The electronic structure specific to the grain boundary will be discussed using a local population and a local density of states (LDOS). The local population in a region α for an eigenstate is defined as

$$P_{i,k}^{\alpha}=\int_{\alpha}|\varphi_{i,k}(\mathbf{r})|^2\,d\mathbf{r}, \tag{1}$$

where $\varphi_{i,k}^{\alpha}(\mathbf{r})$ indicates the wave function for the *i*th eigenstate at the *k*th **k** point. Since the wave function is normalized, $P_{i,k}^{\alpha}$ ranges from 0 to 1. A larger population indicates that the localization of an electronic state on a region is higher. We classified the boundary supercells into two regions, the ''grain-boundary region'' where the boundary core exists and the other which is called the ''quasibulk region,'' as will be shown later in Fig. 3. These regions were chosen to be half in volume, respectively. The local populations were calculated by numerical integration using 64 $\times 128 \times 128$ mesh points in respective regions. The LDOS was obtained by substituting Gaussian functions of 0.5 eV FWHM for the local populations at respective electronic states.

III. RESULTS AND DISCUSSION

A. Atomic structure and energetics

Figure 3 shows equilibrium boundary geometries calculated by the *ab initio* method. For both the boundaries, all the deviations of the atomic positions from the basal planes are less than 0.2 Å in the $[000\bar{1}]$ direction. The basal planes can therefore be regarded as continuous across the interfaces.

The calculated geometries are very similar to the initial ones made by the empirical method. The translation states are kept unchanged through the geometry optimization. The atomic structure of these boundaries can therefore be dealt with qualitatively by the empirical potentials. Quantitatively speaking, however, atomic positions are slightly different. For boundary *A*, the positions of the atoms composing four-fold channels are relaxed by 0.14 Å at maximum from the initial configuration. For boundary *B*, the atoms with dangling bonds showed the largest relaxation: the Zn atoms have moved toward the bulk region by 0.08 Å, whereas the O atoms toward the open channels by 0.18 Å. In the resultant local geometry, the Zn atoms are located closer to the bulk region by 0.25 Å. This behavior is similar to surface rumpling in which smaller cations relax more inwardly than larger anions on the surface. For the $(10\bar{1}0)$ surface of ZnO, rumpling features have been recognized both experimentally and theoretically: Duke *et al.*[57,58] have reported that the amounts of the relaxation for the Zn and O atoms are different by 0.2–0.4 Å on the basis of the analysis of low-energy

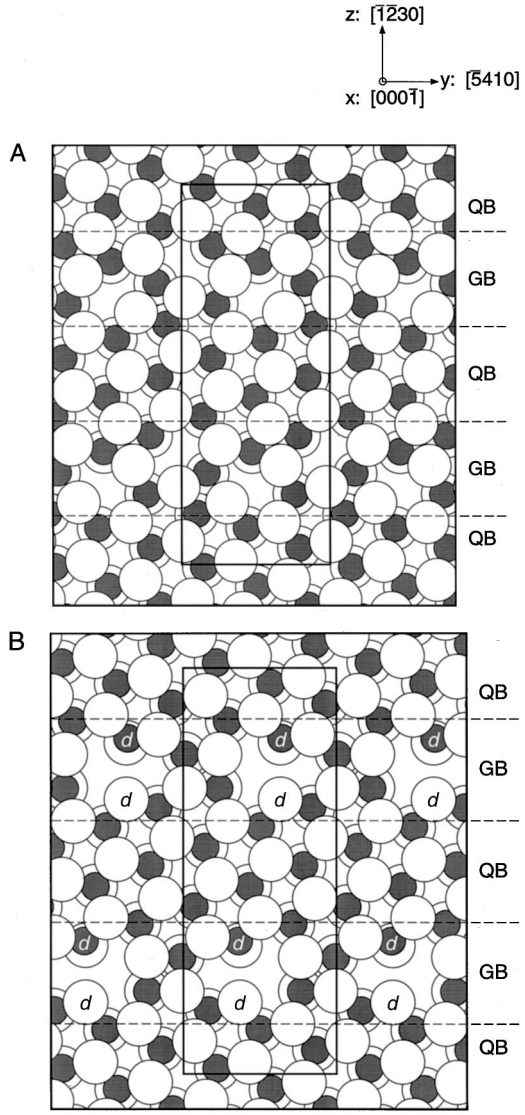

FIG. 3. Equilibrium boundary geometries calculated by the *ab initio* method. The filled and open circles denote Zn and O atoms, respectively. The inner frame indicates the 80-atom supercell. Borders between the grain-boundary (GB) and quasibulk (QB) regions are shown with dotted lines. Atoms possessing dangling bonds are labeled with *d*.

electron diffraction patterns, while Schröer, Krüger, and Pollmann[59] and Jaffe, Harrison, and Hess[60] have reported the differences of 0.12 and 0.075–0.09 Å through *ab initio* LDA and Hartree-Fock calculations, respectively. The difference of 0.25 Å in the present boundary *B* is slightly larger than the calculated values for the surface.

Grain-boundary energies calculated by the *ab initio* and the empirical methods are listed in Table II. To investigate the cell size dependence, empirical calculations were performed for supercells of three sizes. Even for the largest 304-atom cells, the resultant boundary energies are slightly different from our previous results obtained by the calculation under two-dimensional periodic boundary conditions, 1.37 and 1.48 J/m^2 for boundaries *A* and *B*, respectively.[25] This should be due to the difference in cell size and/or boundary conditions.

TABLE II. Grain-boundary energies calculated by the *ab initio* and the empirical methods.

	Grain boundary energy (J/m^2)	
	Boundary *A*	Boundary *B*
Ab initio (80-atom cell)	1.45	1.42
Empirical (80-atom cell)	1.76	1.71
Empirical (192-atom cell)	1.54	1.59
Empirical (304-atom cell)	1.51	1.47

The *ab initio* results show that the energies of boundaries *A* and *B* are nearly the same. This tendency is common to all the empirical results for the supercells with respective sizes. Although the empirical results suggest that the boundary energies have not fully converged with respect to cell size for the 80-atom supercells, boundaries *A* and *B* are likely to have similar boundary energies within the *ab initio* method used in the present study.

Comparing the results for the 80-atom supercells, the boundary energies calculated by the empirical method are not so much different from the results by the *ab initio* method. The grain boundaries in ZnO are likely to be dealt with fairly well in energy by the empirical method based on the fully ionic model, as well as in geometry. This may be due to considerable ionicity of ZnO, which was also suggested by the distribution of the valence charge density.

Table III summarizes the distribution of the bond lengths and angles for the first and the second nearest neighbors in the grain-boundary supercells. For the second nearest neighbors, atom pairs which give the bond length of less than 3.5 Å are chosen. The bond properties for the bulk ZnO, where two types of bonds are present for the first and the second nearest neighbors, respectively, are also shown for comparison.

Regarding the first nearest neighbors, the average of bond lengths in boundary *A* deviates from the bulk average more than that of boundary *B*. Likewise, the standard deviation, i.e., the deviation from the average, is larger. This tendency in standard deviation is also recognized for the bond angles and the bond lengths between the second nearest neighbors although the averages are not so much different between boundaries *A* and *B*. At the core of boundary *A*, the large distortion of the bonds between the first nearest neighbors is required to preserve the complete fourfold coordination. The lengths and the angles are thus disturbed by 10.3% and 33.1% at maxima relative to the bulk averages, respectively. In addition, the second nearest neighbors of like sign are forced to be very close to each other around the fourfold channels: the bond lengths are reduced by 22.9% at maximum.

Boundary *B* also has fourfold channels at the boundary core but the number is a half of that for boundary *A*. The atoms composing the fourfold channels show similar bond distortions to those in boundary *A*. The bonds associated with the atoms possessing dangling bonds are also different

TABLE III. The distribution of bond lengths and angles for the first and the second nearest neighbors (NN's). For the bulk, the number of bonds with a length or an angle is shown in parentheses.

			Boundary *A*	Boundary *B*	Bulk
1st NN	Length (Å)	Average	1.980	1.971	1.966
		Minimum	1.844	1.867	1.964 (3)
		Maximum	2.171	2.040	1.972 (1)
		Standard deviation	0.053	0.038	0.004
	Angle (deg)	Average	109.0	109.2	109.5
		Minimum	73.2	82.2	108.7 (3)
		Maximum	144.2	140.9	110.2 (3)
		Standard deviation	10.2	7.6	0.8
2nd NN	Length (Å)	Average	3.207	3.203	3.210
		Minimum	2.476	2.672	3.198 (6)
		Maximum	3.478	3.384	3.221 (6)
		Standard deviation	0.149	0.110	0.012

from the bonds in the bulk. The bond lengths between the first nearest neighbors are 2.1–5.1 % shorter than the bulk average. The 5.1% is the largest deviation in this geometry. Except for the contributions of the atoms composing the fourfold channels and the atoms possessing dangling bonds, the bond distortion is very small in boundary *B*, as can be recognized in Fig. 3. The small bond distortion should be favorable in reducing the boundary energy. On the other hand, some energy penalty must have been paid due to the presence of the dangling bonds. The balance of the two contributions in opposite sign may have resulted in nearly the same boundary energy as that of boundary *A*.

Thus, the equilibrium core structures with and without dangling bonds are suggested to be present with similar energies in the $\Sigma=7$ boundary of ZnO. Although there has been no experimental observation for the $\Sigma=7$ boundary as far as we know, an analogy in atomic arrangement can be found between the present boundaries and other tilt boundaries in literature. Kiselev *et al.* have reported high-resolution images of the [0001] $\Sigma=13$ boundary in a ZnO bicrystal.[9] They found some types of core structures in the tilt boundary. The core structures are constructed by a sequence of channels with coordination numbers close to six. In the present results, the core structure of boundary *A* is also constructed by a sequence of channels. An important difference is that there are only the channels with even coordination numbers in boundary *A*, whereas a number of fivefold- and sevenfold-coordinated channels are recognized in the high-resolution images reported by Kiselev *et al.* The odd coordination number is inconsistent with the ionic nature of ZnO since it means that at least two first nearest neighbors of like sign are present per channel. We cannot clearly explain the observation of such many odd coordination numbers at the present moment. It may be significant for the observed structures to take atomic displacement along the [0001] direction into account: if the displacement is indeed large, the actual coordination number can be even for the channels whose coordination numbers look odd from the [0001] direction.

A core structure with large open channels and dangling bonds has been observed in the [001]/(310) $\Sigma=5$ symmetric tilt boundary of NiO by Merkle and Smith.[4] Likewise, atomistic simulations on the $\Sigma=5$ boundaries in NiO and MgO have suggested that core structures with large open channels and dangling bonds have the lowest boundary energies at the ground state although the calculated structures are somewhat different from the observed one.[11,16,18,21]

In the present study on the grain boundary of ZnO, a similar core structure is obtained as one of the equilibrium configurations with the lowest boundary energies. The equilibrium core structures with dangling bonds have also been recognized for the tilt boundaries in TiO_2 and Al_2O_3.[6,7,10,14,23] The energy gain by vanishing dangling bonds may not necessarily be dominant in determining boundary energy for metal oxides with ionicity. In ionic materials, it should be quite unfavorable in energy to make ions of like sign closer to each other. Since large reconstruction of atomic arrangements should be accompanied by such an energy penalty, core structures with dangling bonds may be favorable at some boundaries rather than being reconstructed largely to vanish dangling bonds. For covalent materials such as Si and SiC, on the other hand, it has been reported that the energy penalty produced by the presence of dangling bonds are so large that atomic arrangements tend to be reconstructed to eliminate dangling bonds.[2,3,61,62] A further systematic study will allow us to elucidate the grain-boundary geometry more clearly in terms of chemical bonding character.

B. Electronic structure

Figure 4 shows the LDOS for the grain-boundary supercells. The grain-boundary and quasibulk regions are chosen to be half in volume, respectively, as shown in Fig. 3. In terms of the number of atoms, however, they are not half since there is volume expansion associated with the presence of the interface: the boundary regions contain 0.47 and 0.46 times the 80 atoms for boundaries *A* and *B*, respectively, and

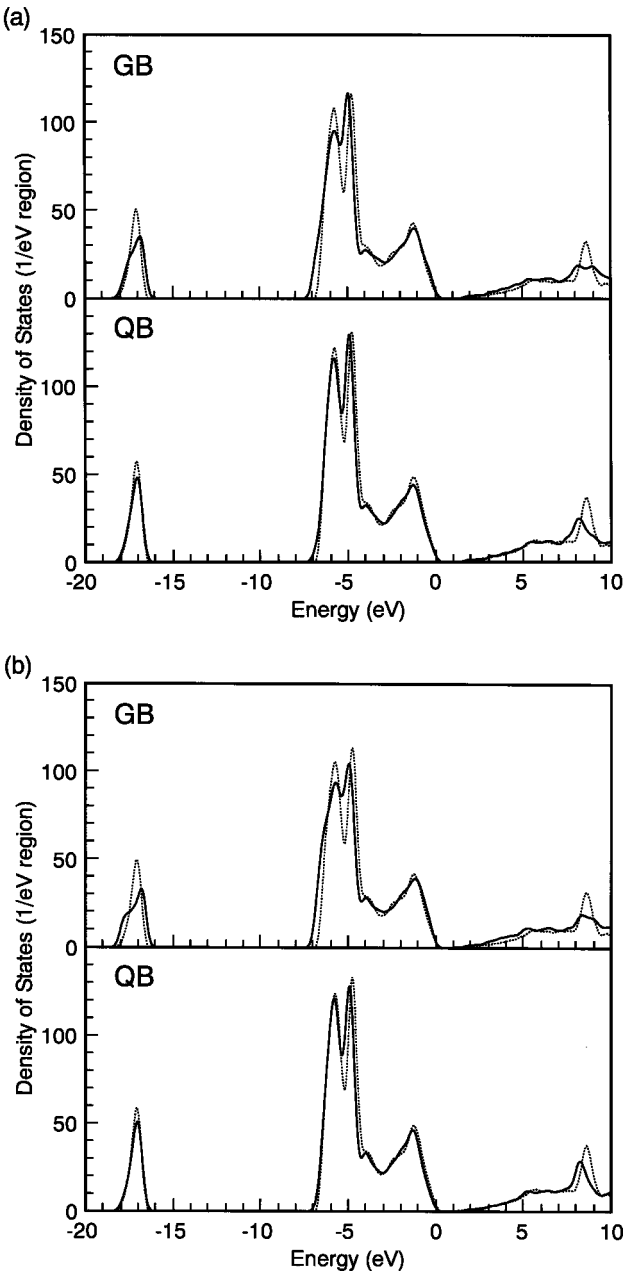

FIG. 4. Local density of states (LDOS) for the supercells of (a) boundary *A* and (b) boundary *B*. The upper and the lower show the LDOS's in the grain-boundary (GB) and quasibulk (QB) regions, respectively. The DOS for the bulk primitive cell is also shown with dotted curves, which is normalized by the number of atoms in each region. The top of the valence band for the bulk primitive cell is chosen as 0 eV. The LDOS's for the boundary supercells are shifted to align the average of the lower valence band in the quasibulk region with that for the bulk primitive cell.

the quasibulk regions contain the rest. In comparison, the DOS for the bulk primitive cell is superimposed on the LDOS's: the bulk DOS is normalized by the number of atoms in each region of the boundary supercells. The shape of the bulk DOS is confirmed to be very similar to the reported LDA results.[25,54,55]

In the bulk ZnO, the lower valence band located at about -17 eV is composed mainly of O $2s$, while the upper valence band situated between -7 and 0 eV is composed mainly of Zn $3d$ and O $2p$. Above the band gap, the unoccupied conduction band is constructed mainly by Zn $4s$ and $4p$. Near the bottom of the conduction band, the density of states is very small due to the large dispersion of the constituent band. For the bulk primitive cell of ZnO, the band gap was calculated to be 0.76 eV. This value is considerably smaller than the experimental one of 3.30 eV.[63] In addition, the peaks associated with Zn $3d$, which is located between -7 and -4 eV, is about 2.5 eV higher in energy than that observed by x-ray photoelectron spectroscopy.[64,65] It has been known that these discrepancies are associated with the LDA.[54,66] Vogel, Krüger, and Pollmann have made LDA calculations including the self-interaction and electronic relaxation corrections.[66] Their results showed that the band gap and the position of the $3d$-associated peaks became much closer to the experimental ones with these corrections. However, the character of the electronic states near the band edges seems not to be affected significantly by the corrections. We therefore believe that the effect of bond disorder on the electronic structure, which is expected to appear mainly at band edges, can be discussed without the corrections.

The LDOS's for the boundary and quasibulk regions in the boundary supercells are somewhat different from each other. In the quasibulk regions, the electronic structure is expected to be similar to that for the bulk. However, the shapes of the LDOS's, especially the peaks located at about 8.5 eV in the conduction band, are slightly affected. This seems to be caused by the small disturbance of atomic arrangements and/or interactions with the boundary regions.

In the boundary regions, the shapes of the LDOS's are flatter in general than those for the LDOS's in the quasibulk regions and the bulk DOS. The lower and upper valence bands are wider. This indicates that the electronic states associated with the grain boundaries are present at the valence band edges. For the conduction band, the density of states in the energy range of about 2–5 eV is slightly higher than that of the bulk. Grain boundary states should form here likewise. It is interesting that these main features in the LDOS's are common to boundaries *A* with large bond distortion and no dangling bonds, and boundary *B* with small bond distortion and some dangling bonds. The bond distortion and the presence of the dangling bonds seem to show similar effects on the shape of the LDOS.

We now focus on the electronic states in the vicinity of the band gap since they are important for the boundary-induced electrical properties of ZnO. The bulk primitive cell exhibited the direct band gap at the Γ point. In other words, the top of the valence band and the bottom of the conduction band were given at the Γ point. This feature was also recognized for both boundaries *A* and *B* supercells. We therefore discuss the electronic states at the Γ point for the boundary supercells. Figure 5 shows the local population in the grain-boundary regions for the electronic states at the Γ point. A larger population indicates that the localization of the electronic state on the boundary region is higher. When electronic states delocalize ideally and/or are constructed equally by the contributions from the grain-boundary and quasibulk

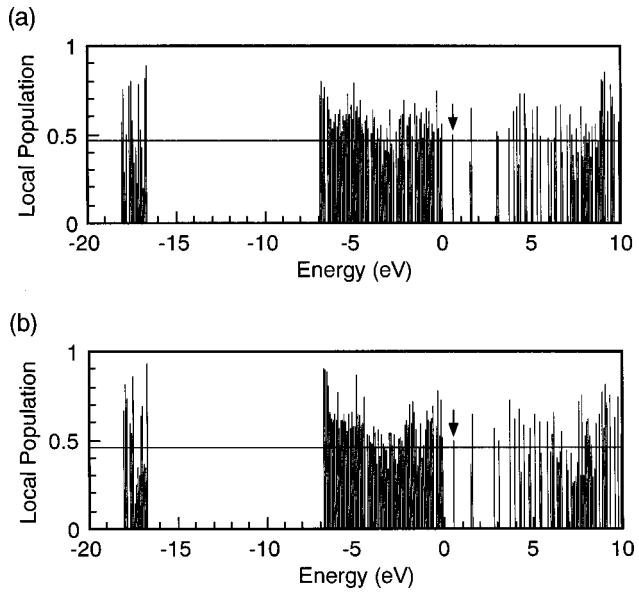

FIG. 5. Local populations in the grain-boundary regions for the electronic states at the Γ point: (a) boundary *A* and (b) boundary *B* supercells. The reference values of the populations, 0.47 and 0.46 for boundaries *A* and *B*, respectively, are shown with horizontal lines. The arrows indicate the bottom of the conduction band.

regions, the local populations should be 0.47 and 0.46 for boundaries *A* and *B*, respectively, on the basis of the number of atoms in the boundary regions. We use these values as references of the local populations. As mentioned above, these are slightly smaller than 0.5 due to the volume expansion normal to the interface.

In the lower valence band situated at about −17 eV, electronic states with large populations, which are constructed mainly by O 2*s* in the grain boundary regions, distribute through the band for both the boundaries. In the upper valence band situated between −7 and 0 eV, electronic states with large populations appear mainly near the band bottom. These states should consist mainly of Zn 3*d* in the boundary regions. The localization is recognized more clearly for the boundary *B*, presumably due to the effects of the dangling-bonds associated with Zn 3*d*. Some states somewhat below the top of the valence band also show large populations for both the boundaries. On the other hand, the local populations at the band top, 0.56 and 0.53 for boundaries *A* and *B*, respectively, deviate only slightly from the reference values. This indicates that the electronic states do not localize significantly on the boundary regions.

In the conduction band, the electronic states with relatively large populations are recognized at about 1 eV above the bottom for both the boundaries. At the bottom, the local populations are 0.51 and 0.50 for boundaries *A* and *B*, respectively. The localization is quite low, as the top of the valence band is.

The features in local population were very similar at the other **k** points: for both boundaries, electronic states localizing highly on the boundary regions appear mainly in the lower valence band and near the bottom of the upper valence band. Likewise, the electronic states closest to the top of the valence band or the bottom of the conduction band do not localize significantly on the boundary regions. In the vicinity of the band gap, the shape of the LDOS's is therefore very similar to that of the bulk DOS although the apparent band gaps, 0.60 and 0.67 eV for boundary *A* and *B* supercells, respectively, are slightly smaller than the bulk gap of 0.76 eV. Deep interfacial electronic states are not recognized even for the boundary *B* with dangling bonds.

For the $(10\bar{1}0)$ surface of ZnO, specific states have been reported to form at both the edges of the lower valence band and the bottom of the upper valence band,[59] as is the case with the boundaries dealt with in the present study. For the surface, a state associated with O 2*p* dangling bonds has also been reported to appear slightly above the top of the upper valence band. In the present study, such a state is not clearly recognized for boundary *B* with dangling bonds: localized states associated with O 2*p* dangling bonds seem to form somewhat below the top of the upper valence band. Since the Zn and O atoms with dangling bonds face each other across the open channels in the boundary geometry, the effect of the dangling bonds may be reduced.

For the surface, it has also been reported that the electronic structure near the conduction band bottom is very similar to that of the bulk. This feature is common to the boundaries in the present study. The conduction band in ZnO seems not to be significantly affected by the bond disorder at the surface and interfaces.

In order to understand the character of the conduction band, the spatial distribution of the wave function at the conduction-band bottom is investigated. Figure 6 shows contour plots for the square of the absolute value of the wave function on the (0001) Zn plane. For the perfect crystal of ZnO, a calculation based on the linear combination of atomic orbitals (LCAO) suggested that the conduction-band bottom is constructed mainly by bonding interactions among Zn 4*s* orbitals.[67] The relatively high values among the Zn atoms in Fig. 6(a) also indicate the bonding character. The interactions among Zn 4*s* orbitals are very large at the bottom of the conduction band, which can be understood by the large dispersion of the constituent band or the small density of states shown in Fig. 4. In other words, the electronic state at the conduction band bottom is considerably delocalized.

The interactions among Zn 4*s* orbitals are also recognized in the quasibulk regions for the boundary supercells. In the boundary regions, moreover, the hybridization of *p* and *d* characteristics into the *s* characteristic is obvious. For boundary *A* [Fig. 6(b)], such characteristics are recognized for almost all the Zn atoms composing the fourfold- and/or eightfold-coordinated channels. The values of the wave function are relatively high at these parts. For boundary *B* [Fig. 6(c)], the hybridization for the Zn atoms composing the fourfold-coordinated channels is similar to the case of the boundary *A*. In addition, the Zn atoms possessing dangling bonds show *s*-*p* hybridized characteristics, spreading toward the open channels. Thus, *s*-*p* and/or *s*-*d* hybridized characteristics appear in the boundary regions for both boundaries. The localization of the electronic states on the boundary regions, however, should be low since the local populations deviate only slightly from the reference values as discussed

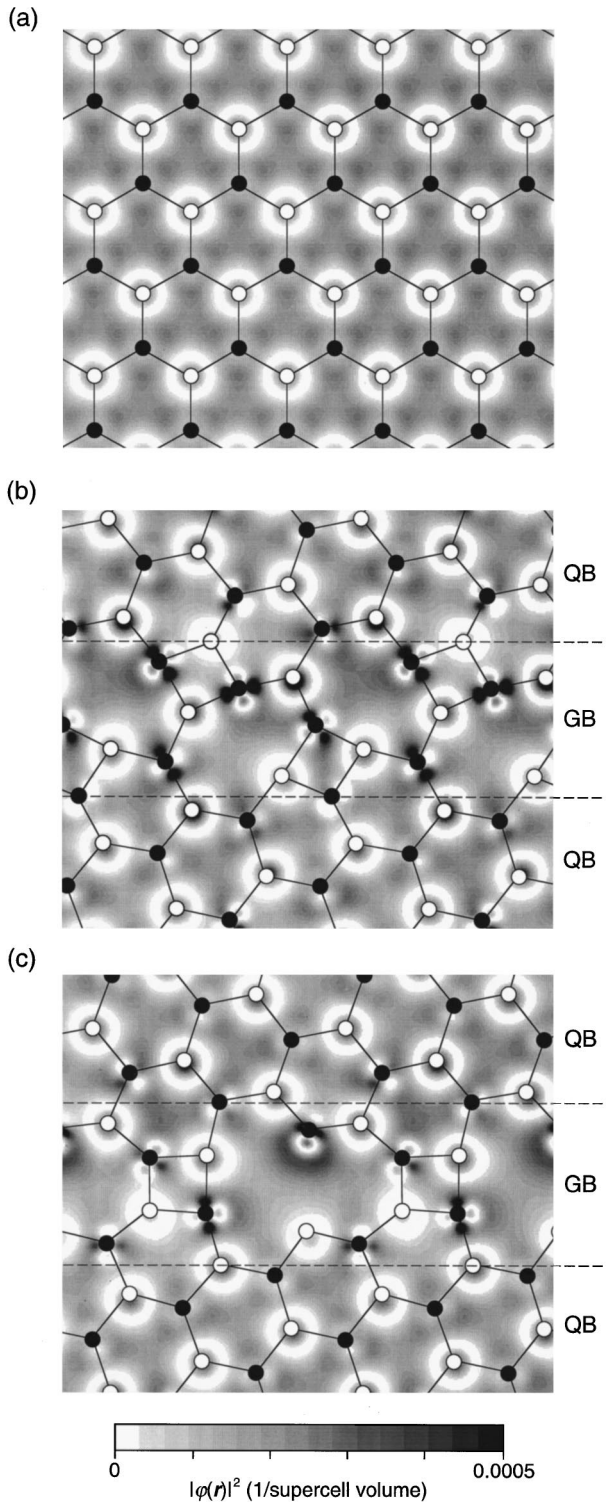

FIG. 6. Spatial distribution of the wave function at the bottom of the conduction band for (a) the bulk primitive cell and (b) boundary *A* and (c) boundary *B* supercells. The contours for the square of the absolute value of the wave function, $|\varphi(\mathbf{r})|^2$, are plotted on the (0001) Zn plane. The thickest contour also indicates the values between 0.0005 and 0.0012 (1/supercell volume). For the bulk, the $|\varphi(\mathbf{r})|^2$ is normalized by the number of atoms in the boundary supercells (80 atoms). The filled circles denote the positions of the Zn atoms on the Zn plane. The open circles denote the positions of the O atoms which are located on the $(000\bar{1})$ O plane adjacent to the Zn plane.

above. This is presumably due to the domination of the Zn 4*s* character at the bottom of the conduction band. Since the interaction among *s* orbitals is not very sensitive to bond angles in general, the distortion of the angles in the boundary geometries may not have affected the electronic state significantly. In addition, the effect of the dangling bonds on the electronic state seems to be small, presumably due to the delocalized character.

Thus, the effects of the bond disorder are very small for the electronic states in the vicinity of the band gap, especially for that at the bottom of the conduction band. This can be generally explained by the band structure intrinsic to ZnO as follows.

For covalent materials such as Si, Ge, and SiC, the valence band is constructed mainly by the bonding interactions between adjacent atoms, while the conduction band by the antibonding interactions. In this case, bond distortion and the presence of dangling bonds have the potential to generate electronic states in the band gap since these effects tend to diminish or vanish the splitting between the bonding and antibonding states. In practice, it has been reported that bond disorder induces highly localized electronic states around the top of the valence band and the bottom of the conduction band for tilt and twist boundaries in Si, Ge, and SiC,[62,68–71] and that such electronic states can be deep in the band gap when bond distortion is large and/or dangling bonds are present.[68–71]

For ZnO, its ionicity should make the valence and conduction bands consist of the interactions among like atoms in addition to the interactions between Zn and O atoms. If the former feature dominates, bond distortion and the presence of dangling bonds do not necessarily induce electronic states in the band gap: the localized electronic states associated with the bond disorder should tend to form within the valence or conduction band. Considering the electronic structure of the boundaries dealt with in the present study and the $(10\bar{1}0)$ surface reported by Schröer, Krüger, and Pollmann,[59] such a feature is likely to be strong, especially in the conduction band. In other words, the small effects of the bond disorder in the vicinity of the band gap can be attributed to such band structure of ZnO.

For the grain boundaries in other oxides such as Al_2O_3, TiO_2, and $SrTiO_3$, it has been reported that deep electronic states do not form either, although localized states have been recognized at the valence- and/or conduction-band edges for the boundaries of Al_2O_3 and TiO_2.[22–24] This behavior may also be attributed to the band structures with some ionicity in metal oxides. For the grain boundaries of ZnO dealt with in the present study, the effects of the bond disorder on the conduction-band bottom is much smaller than those in the above-noted oxides. This should be due to much higher delocalization of the conduction band in ZnO.

Thus, the absence of deep electronic states at the grain boundaries can be generally explained by the band structure intrinsic to ZnO. Bond disorder at the grain boundaries is therefore unlikely to result in the generation of deep electronic states even if arbitrary boundaries are investigated. In ZnO varistors, deep interfacial states have been observed at 0.6–1.0 eV below the bottom of the conduction band.[31–35]

The present results suggest that such deep states are unlikely to originate solely from bond disorder at the grain boundaries when the stoichiometry is preserved. The roles of native defects and/or impurities segregating at the grain boundaries should therefore be significant for the boundary-induced electrical properties of ZnO varistors.

IV. CONCLUSION

We have investigated the atomic and electronic structure of the $[0001]/(\overline{1}\,2\,3\,0)$ $\Sigma=7$ symmetric tilt boundary in ZnO by an *ab initio* plane-wave pseudopotential method. Two types of the equilibrium geometries are obtained with similar boundary energies. The atomic arrangement is largely reconstructed to vanish dangling bonds in one configuration. The other shows small bond distortion but has four dangling bonds per unit boundary area. The balance between the energies for deforming atomic arrangements and vanishing dangling bonds should be significant in determining the boundary energy.

Regarding the electronic structure, localized grain-boundary states form mainly at the lower valence band and the bottom of the upper valence band due to the bond distortion and/or the presence of the dangling bonds. On the other hand, the electronic states in the vicinity of the band gap are not significantly affected by the bond disorder. Deep electronic states are not generated in the band gap even for the configuration with dangling bonds. This behavior can be generally explained by the band structure intrinsic to ZnO. The deep interface states observed in ZnO varistors should therefore not originate solely from bond disorder at stoichiometric boundaries. Native defects and/or impurities segregating at the grain boundaries should play central roles for the boundary-induced electrical properties.

ACKNOWLEDGMENT

This work was performed through the ACT program of the Japan Science and Technology Corporation, and Special Coordination Funds of the Science and Technology Agency of the Japanese Government.

[1] D. G. Brandon, B. Ralph, S. Ranganathan, and M. S. Wald, Acta Metall. **12**, 813 (1964).
[2] J. Thibault, J. L. Rouviere, and A. Bourret, in *Materials Science and Technology*, edited by R. W. Cahn, P. Haasen, and E. J. Kramer (VCH, Weinheim, 1991), Vol. 4, p. 321.
[3] K. Tanaka and M. Kohyama, in *Electron Microscopy 1998*, edited by H. A. C. Benavides and M. J. Yacamán (Institute of Physics, Bristol, 1998), Vol. 2, p. 581.
[4] K. L. Merkle and D. J. Smith, Phys. Rev. Lett. **59**, 2887 (1987).
[5] K. L. Merkle, J. F. Reddy, C. L. Wiley, and D. J. Smith, J. Phys. (Paris), Colloq. **49**, C5-251 (1988).
[6] T. Höche, P. R. Kenway, H.-J. Kleebe, M. Rühle, and P. A. Morris, J. Am. Ceram. Soc. **77**, 339 (1994).
[7] U. Dahmen, S. Paciornik, I. G. Solorzano, and J. B. Vandersande, Interface Sci. **2**, 125 (1994).
[8] N. D. Browning and S. J. Pennycook, J. Phys. D **29**, 1779 (1996).
[9] A. N. Kiselev, F. Sarrazit, E. A. Stepantsov, E. Olsson, T. Claeson, V. I. Bondarenko, R. C. Pond, and N. A. Kiselev, Philos. Mag. A **76**, 633 (1997).
[10] W.-Y. Lee, P. D. Bristowe, I. G. Solorzano, and J. B. Vandersande, in *Defect-Interface Interactions*, edited by E. P. Kvam, A. H. King, M. J. Mills, T. D. Sands, and V. Vitek, MRS Symposium Proceedings No. 319 (Materials Research Society, Pittsburgh, 1994), p. 239.
[11] D. M. Duffy and P. W. Tasker, Philos. Mag. A **47**, 817 (1983).
[12] D. M. Duffy and P. W. Tasker, Philos. Mag. A **48**, 155 (1983).
[13] P. W. Tasker and D. M. Duffy, Philos. Mag. A **47**, L45 (1983).
[14] P. R. Kenway, J. Am. Ceram. Soc. **77**, 349 (1994).
[15] A. P. Sutton and R. W. Balluffi, *Interfaces in Crystalline Materials* (Oxford University Press, New York, 1995), p. 318.
[16] D. J. Harris, G. W. Watson, and S. C. Parker, Philos. Mag. A **74**, 407 (1996).
[17] W. Wunderlich, Phys. Status Solidi A **170**, 99 (1998).
[18] Y. Yan, M. F. Chisholm, G. Duscher, A. Maiti, S. J. Pennycook, and S. T. Pantelides, Phys. Rev. Lett. **81**, 3675 (1998).
[19] M. Nomura, N. Ichinose, K. Yamaji, H. Haneda, and J. Tanaka, J. Electroceram. **4**, 91 (1999).
[20] H. S. Domingos and P. D. Bristowe, Scr. Mater. **41**, 1347 (1999).
[21] T. E. Karakasidis and M. Meyer, Modell. Simul. Mater. Sci. Eng. **8**, 117 (2000).
[22] S. D. Mo, W. Y. Ching, and R. H. French, J. Am. Ceram. Soc. **79**, 627 (1996).
[23] I. Dawson, P. D. Bristowe, M. H. Lee, M. C. Payne, M. D. Segall, and J. A. White, Phys. Rev. B **54**, 13 727 (1996).
[24] S. D. Mo, W. Y. Ching, M. F. Chisholm, and G. Duscher, Phys. Rev. B **60**, 2416 (1999).
[25] F. Oba, I. Tanaka, S. R. Nishitani, H. Adachi, B. Slater, and D. H. Gay, Philos. Mag. A **80**, 1567 (2000).
[26] D. R. Clarke, J. Am. Ceram. Soc. **82**, 485 (1999).
[27] M. Matsuoka, Jpn. J. Appl. Phys. **10**, 736 (1971).
[28] K. Mukae, K. Tsuda, and I. Nagasawa, Jpn. J. Appl. Phys. **16**, 1361 (1977).
[29] G. E. Pike and C. H. Seager, J. Appl. Phys. **50**, 3414 (1979).
[30] G. E. Pike, S. R. Kurtz, P. L. Gourley, H. R. Philipp, and L. M. Levinson, J. Appl. Phys. **57**, 5512 (1985).
[31] J. P. Gambino, W. D. Kingery, G. E. Pike, H. R. Philipp, and L. M. Levinson, J. Appl. Phys. **61**, 2571 (1987).
[32] K. Tsuda and K. Mukae, J. Ceram. Soc. Jpn. **97**, 1211 (1989).
[33] T. Maeda, S. Meguro, and M. Takata, Jpn. J. Appl. Phys., Part 2 **28**, L714 (1989).
[34] R. A. Winston and J. F. Cordaro, J. Appl. Phys. **68**, 6495 (1990).
[35] K. Tsuda and K. Mukae, J. Ceram. Soc. Jpn. **100**, 1239 (1992).
[36] Y. Yano, Y. Takai, and H. Morooka, J. Mater. Res. **9**, 112 (1994).
[37] S. Fujitsu, K. Koumoto, and H. Yanagida, Solid State Ionics **32/33**, 482 (1989).
[38] M. Yodogawa, Y. Ikuhara, F. Oba, and I. Tanaka, Key Eng. Mater. **157-158**, 24 (1999).

[39] F. Oba, I. Tanaka, and H. Adachi, Jpn. J. Appl. Phys., Part 1 **38**, 3569 (1999).
[40] E. Sonder, M. M. Austin, and D. L. Kinser, J. Appl. Phys. **54**, 3566 (1983).
[41] S. Fujitsu, H. Toyoda, and H. Yanagida, J. Am. Ceram. Soc. **70**, C71 (1987).
[42] K. Tsuda and K. Mukae, J. Ceram. Soc. Jpn. **97**, 1211 (1989).
[43] F. Stucki and F. Greuter, Appl. Phys. Lett. **57**, 446 (1990).
[44] F. Oba, H. Adachi, and I. Tanaka, J. Mater. Res. **15**, 2167 (2000).
[45] J. R. Chelikowsky and M. L. Cohen, in *Handbook on Semiconductors*, edited by P. T. Landsberg (Elsevier, North-Holland, 1992), Vol. 1, p. 59.
[46] J. P. Perdew and A. Zunger, Phys. Rev. B **23**, 5048 (1981).
[47] M. C. Payne, M. P. Teter, D. C. Allan, T. A. Arias, and J. D. Joannopoulos, Rev. Mod. Phys. **64**, 1045 (1992).
[48] M. Kohyama, Modell. Simul. Mater. Sci. Eng. **4**, 397 (1996).
[49] R. P. Feynman, Phys. Rev. **56**, 340 (1939).
[50] N. Troullier and J. L. Martins, Phys. Rev. B **43**, 1993 (1991).
[51] L. Kleinman and D. M. Bylander, Phys. Rev. Lett. **48**, 1425 (1982).
[52] D. J. Chadi and M. L. Cohen, Phys. Rev. B **8**, 5747 (1973).
[53] S. C. Abrahams and J. L. Bernstein, Acta Crystallogr., Sect. B: Struct. Crystallogr. Cryst. Chem. **25**, 1233 (1969).
[54] P. Schröer, P. Krüger, and J. Pollmann, Phys. Rev. B **47**, 6971 (1993).
[55] Y. N. Xu and W. Y. Ching, Phys. Rev. B **48**, 4335 (1993).
[56] G. V. Lewis and C. R. A. Catlow, J. Phys. C **18**, 1149 (1985).
[57] C. B. Duke, A. R. Lubinsky, S. C. Chang, B. W. Lee, and P. Mark, Phys. Rev. B **15**, 4865 (1977).
[58] C. B. Duke, R. J. Meyer, A. Paton, and P. Mark, Phys. Rev. B **18**, 4225 (1978).
[59] P. Schröer, P. Krüger, and J. Pollmann, Phys. Rev. B **49**, 17 092 (1994).
[60] J. E. Jaffe, N. M. Harrison, and A. C. Hess, Phys. Rev. B **49**, 11 153 (1994).
[61] M. Kohyama and R. Yamamoto, Phys. Rev. B **49**, 17 102 (1994).
[62] M. Kohyama, Philos. Mag. Lett. **79**, 659 (1999).
[63] V. Srikant and D. R. Clarke, J. Appl. Phys. **83**, 5447 (1998).
[64] W. Göpel, J. Pollmann, I. Ivanov, and B. Reihl, Phys. Rev. B **26**, 3144 (1982).
[65] S. V. Didziulis, S. L. Cohen, K. D. Butcher, and E. I. Solomon, Inorg. Chem. **27**, 2238 (1988).
[66] D. Vogel, P. Krüger, and J. Pollmann, Phys. Rev. B **54**, 5495 (1996).
[67] F. Oba, I. Tanaka, and H. Adachi (unpublished).
[68] M. Kohyama and R. Yamamoto, Phys. Rev. B **50**, 8502 (1994).
[69] M. Kohyama and R. Yamamoto, in *Amorphous Silicon Technology 1993*, edited by E. A. Schiff, M. J. Thompson, A. Madan, K. Tanaka, and P. G. LeComber, MRS Symposium Proceedings No. 297 (Materials Research Society, Pittsburgh, 1993), p. 177.
[70] E. Tarnow, T. Arias, P. D. Bristowe, P. Dallot, G. P. Francis, J. D. Joannopoulos, and M. C. Payne, in *Atomic Scale Calculations of Structure in Materials*, edited by M. S. Daw and M. A. Schlüter, MRS Symposium Proceedings No. 193 (Materials Research Society, Pittsburgh, 1990), p. 235.
[71] E. Tarnow, P. Dallot, P. D. Bristowe, J. D. Joannopoulos, G. P. Francis, and M. C. Payne, Phys. Rev. B **42**, 3644 (1990).